JOURNAL OF GUIDANCE, CONTROL, AND DYNAMICS
Vol. 37, No. 5, September–October 2014

Engineering Notes

Lyapunov-Based Adaptive Feedback for Spacecraft Planar Relative Maneuvering via Differential Drag

David Pérez* and Riccardo Bevilacqua†
Rensselaer Polytechnic Institute, Troy, New York 12180

DOI: 10.2514/1.G000191

I. Introduction

In 1989, Leonard et al. [1] introduced the concept of using differential drag at low Earth orbits (LEOs) for propellantless in-plane spacecraft relative motion control. This method consists of varying the aerodynamic drag experienced by different spacecraft, by opening or closing a set of drag surfaces, or varying the attitude of asymmetrical spacecraft, thus generating differential accelerations between them. Since there is no propellant exhaust and no plume impingement, highly sensitive onboard sensors may operate in a cleaner environment. Moreover, since the relative accelerations generated by the drag forces are small, equipment sensitive to shocks or vibrations may benefit from the use of differential drag, assuming that drag control devices operate without exciting vibration modes of the spacecraft.

The main limitation of using differential drag for relative motion control is that one must operate at a relatively low LEO. In this regime, differential drag forces can be made large enough to achieve effective control. However, this increased drag force results in faster orbit decay, and thus a more limited mission life. However, these formation-flying orbits are of interest since they can be used for communications, astronomical, atmospheric, and Earth observation applications [2,3].

In this work, a chaser and a target spacecraft are considered. The reference frame commonly used for spacecraft relative motion is the local-vertical/local-horizontal (LVLH) reference frame, centered at the target spacecraft, where x points from Earth to the target spacecraft, y points along the track of the target spacecraft, and z completes the right-handed frame. The state of the system consists of the position and velocity, in the LVLH frame, of the chaser spacecraft relative to the target spacecraft.

Atmospheric differential drag is projected on the alongtrack direction and can provide effective control only in the orbital plane (x and y). The control law is based on the assumption that the control is either positive maximum (+1), which implies chaser maximizing (opening) its drag surface and target minimizing (closing) it; negative maximum (−1), which implies chaser maximizing (opening) its drag surface and target minimizing (closing) it; or zero (0), which implies same surface on chaser and target: that is, no differential acceleration, as previously done in [4–6].

In previous work [7], a Lyapunov controller was developed for maneuvering using differential drag. An analytical expression for the magnitude of the differential drag acceleration that ensures stability was also found. Partial derivatives of this critical value in terms of $\underline{\boldsymbol{Q}}$ (Lyapunov equation matrix) and $\underline{\boldsymbol{A}}_d$ (reference linear dynamics matrix) were presented in [8,9] for the case in which the controller acts as a regulator. Furthermore, an adaptation that chooses an appropriate positive definite matrix $\underline{\boldsymbol{P}}$ in a quadratic Lyapunov function, by modifying the $\underline{\boldsymbol{Q}}$ and $\underline{\boldsymbol{A}}_d$ matrices based on the partial derivatives, was developed. Nonetheless, the adaptation was limited to regulation maneuvers, since the partial derivatives were developed for that case only.

The foremost contribution of this work consists of the complete analytical expressions for the mentioned partial derivatives for the general case in which the spacecraft are tracking a linear reference model, which can also be used for tracking a guidance trajectory or a desired final state (regulation). Simulations validate the adaptive Lyapunov controller for a fly-around maneuver followed by a long-term formation-keeping period and a rendezvous maneuver via the Systems Tool Kit (STK®). An assessment of the performances of the designed adaptive Lyapunov controller and a comparison versus a nonadaptive Lyapunov controller [7] are shown.

II. Linear Reference and Nonlinear Models

The linear reference model is obtained by stabilizing the Schweighart and Sedwick dynamics [10] using a linear quadratic regulator (LQR). The resulting model is represented by

$$\dot{\boldsymbol{x}}_d = \underline{\boldsymbol{A}}_d \boldsymbol{x}_d + \boldsymbol{B}u_d, \qquad \underline{\boldsymbol{A}}_d = \underline{\boldsymbol{A}} - \boldsymbol{B}\boldsymbol{K}, \qquad u_d = \boldsymbol{K}x_t \tag{1}$$

where $\boldsymbol{x} = [x \quad y \quad \dot{x} \quad \dot{y}]^T$, $\boldsymbol{K}$ is a constant vector found by solving the LQR problem, $\boldsymbol{x}_t$ is the desired guidance, $\underline{\boldsymbol{A}}$ is the state matrix from the Schweighart and Sedwick dynamics [10], $\boldsymbol{x}_d$ is the desired reference dynamics tracking the guidance, and $\boldsymbol{B} = [0 \quad 0 \quad 0 \quad 1]^T$.

The nonlinear relative motion dynamics used for the development of the controller is expressed as

$$\dot{\boldsymbol{x}} = \begin{bmatrix} \underline{0}_{2\times2} & \underline{\mathbf{I}}_{2\times2} \\ \underline{0}_{2\times2} & \underline{0}_{2\times2} \end{bmatrix}\boldsymbol{x} + \begin{bmatrix} 0 \\ 0 \\ f_x(x,y,\dot{x},\dot{y}) \\ f_y(x,y,\dot{x},\dot{y}) \end{bmatrix} + \begin{bmatrix} 0 \\ 0 \\ 0 \\ a_{D\text{rel}} \end{bmatrix} = f(\boldsymbol{x}) + \begin{bmatrix} 0 \\ 0 \\ 0 \\ a_{D\text{rel}} \end{bmatrix},$$

$$f_x(x,y,\dot{x},\dot{y}) = \mu\left(\frac{1}{\boldsymbol{r}_T^2} - \frac{\boldsymbol{r}_T + x}{((\boldsymbol{r}_T + x)^2 + y^2)^{3/2}}\right) + 2\omega\dot{y} + 2\omega^2 x + a_{J2x}$$

$$f_y(x,y,\dot{x},\dot{y}) = -\mu\left(\frac{y}{((\boldsymbol{r}_T + x)^2 + y^2)^{3/2}}\right) - 2\omega\dot{x} + 2\omega^2 y + a_{J2y} \tag{2}$$

where $\boldsymbol{r}_T$ is the magnitude of the position vector of the target, ω is the angular velocity of the LVLH frame, and a_{J2x} and a_{J2y} are the differential accelerations caused by the J_2 perturbation. Note that f contains the Keplerian nonlinear dynamics and the J_2 perturbation but not the drag acceleration. The goal of using differential drag is to drive the state $\boldsymbol{x}$ to $\boldsymbol{x}_d$ without using propellant.

It should be noted that the adaptive controller uses the truncated nonlinear dynamics representation of Eq. (2) to calculate the critical value and the partial derivatives shown later on in Eqs. (7), (16), and (18). In the simulations, the motion of the spacecraft is modeled using STK's High-Precision Orbit Propagator (HPOP).

Received 30 July 2013; revision received 17 April 2014; accepted for publication 4 May 2014; published online 15 July 2014.

*Postdoctoral Researcher, Mechanical, Aerospace and Nuclear Engineering Department, 110 8th Street; perezd4@rpi.edu. Member AIAA.

†Assistant Professor, Mechanical, Aerospace and Nuclear Engineering Department, 110 8th Street; bevilr@rpi.edu. Member AIAA (Corresponding Author).

III. Adaptive Lyapunov Control

A. Lyapunov Control Law

The Lyapunov function and its time derivative are given by [7]

$$V = \boldsymbol{e}^T \underline{\boldsymbol{P}} e, \qquad \boldsymbol{e} = \boldsymbol{x} - \boldsymbol{x}_d \tag{3}$$

$$\dot{V} = -\mathbf{e}^T \underline{\boldsymbol{Q}} \mathbf{e} + 2\Delta \tag{4}$$

where $\underline{\boldsymbol{P}}$ and $\underline{\boldsymbol{Q}}$ are symmetric positive-definite matrices; $\boldsymbol{e}$ is the tracking error vector; and Δ, β, and δ are given by the following expressions:

$$\Delta = \beta\hat{u} - \delta, \qquad \beta = \mathbf{e}^T \underline{\boldsymbol{P}} \boldsymbol{B} a_{D\text{rel}},$$

$$\delta = \mathbf{e}^T \underline{\boldsymbol{P}}(\underline{\boldsymbol{A}}_d \boldsymbol{x} - \boldsymbol{f}(\boldsymbol{x}) + \boldsymbol{B}u_d), \qquad \hat{u} = \begin{cases} 1 \\ 0 \\ -1 \end{cases} \tag{5}$$

As long as $\Delta < 0$, the nonlinear dynamics will track the desired trajectory. However, the system cannot be guaranteed to be Lyapunov stable if δ is positive and has a higher magnitude than β. The magnitude of β is linearly dependent on $a_{D\text{rel}}$, which indicates that, if $a_{D\text{rel}}$ is too small (i.e., the density and/or the differential in the ballistic coefficients are too small), the system will be unstable.

The control strategy proposed in [7] is used herein [Eq. (6)]. At this stage, it only guarantees that the product $\beta\hat{u}$ is negative:

$$\hat{u} = -\text{sign}(\beta) = -\text{sign}(\boldsymbol{e}^T \underline{\boldsymbol{P}} \boldsymbol{B}) \tag{6}$$

The following section focuses on guaranteeing a negative time derivative of the Lyapunov function.

B. Critical Value for the Differential Drag

An analytical value for the magnitude of the differential drag ensuring Lyapunov stability (critical value) was developed by the authors in [8,9]. The expression for this value is found by imposing $\Delta < 0$ [Eq. (5)]. For the case in which the nonlinear dynamics is tracking the reference dynamics, the expression for the critical value becomes

$$a_{D\text{crit}} = \frac{\boldsymbol{e}^T \underline{\boldsymbol{P}}(\underline{\boldsymbol{A}}_d \boldsymbol{x} - \boldsymbol{f}(\boldsymbol{x}) + \boldsymbol{B}u_d)}{|\boldsymbol{e}^T \underline{\boldsymbol{P}} \boldsymbol{B}|} \tag{7}$$

This expression is also valid for the cases in which the nonlinear dynamics is tracking a guidance trajectory or just being regulated.

C. General Partial Derivatives

Starting from Eq. (7), the critical value is rewritten as

$$a_{D\text{crit}} = \eta(\underline{\boldsymbol{P}})\psi(\underline{\boldsymbol{A}}_d),$$

$$\eta(\underline{\boldsymbol{P}}) = \frac{\boldsymbol{e}^T \underline{\boldsymbol{P}}}{|\boldsymbol{e}^T \underline{\boldsymbol{P}} \boldsymbol{B}|}, \qquad \psi(\underline{\boldsymbol{A}}_d) = \underline{\boldsymbol{A}}_d \boldsymbol{x} - \boldsymbol{f}(\boldsymbol{x}) + \boldsymbol{B}u_d \tag{8}$$

where matrix $\underline{\boldsymbol{P}}$ is a function of matrices $\underline{\boldsymbol{A}}_d$ and $\underline{\boldsymbol{Q}}$ via the following Lyapunov equation:

$$-\underline{\boldsymbol{Q}} = \underline{\boldsymbol{A}}_d^T \underline{\boldsymbol{P}} + \underline{\boldsymbol{P}} \underline{\boldsymbol{A}}_d \tag{9}$$

which, as shown in [11], can be rewritten as

$$\boldsymbol{P}_v = -\underline{\boldsymbol{A}}_v{}^{-1} \boldsymbol{Q}_v,$$

$$\underline{\boldsymbol{A}}_v = \underline{\mathbf{I}}_{4\times4} \otimes \underline{\boldsymbol{A}}_d + \underline{\boldsymbol{A}}_d \otimes \underline{\mathbf{I}}_{4\times4}, \quad \boldsymbol{P}_v = \text{vec}(\underline{\boldsymbol{P}}), \quad \boldsymbol{Q}_v = \text{vec}(\underline{\boldsymbol{Q}}) \tag{10}$$

In [8,9], the partial derivatives of $\underline{\boldsymbol{P}}$ in terms of $\underline{\boldsymbol{A}}_d$ and $\underline{\boldsymbol{Q}}$ were found; these derivatives are used in the following developments and can be expressed as

$$\frac{\partial \underline{\boldsymbol{P}}}{\partial \underline{\boldsymbol{A}}_d} = T_2\left(\left[T_3^{-1}\left(\frac{\partial \underline{\boldsymbol{A}}_v}{\partial \underline{\boldsymbol{A}}_d}\right) \otimes \underline{\mathbf{I}}_{16\times16}\right]\left[\underline{\mathbf{I}}_{4\times4} \otimes T_1^{-1}\left(\frac{\partial \boldsymbol{P}_v}{\partial \underline{\boldsymbol{A}}_v}\right)\right]\right)$$

$$\frac{\partial \underline{\boldsymbol{A}}_v}{\partial \underline{\boldsymbol{A}}_d} = (\underline{\mathbf{I}}_{4\times4} \otimes \underline{\boldsymbol{U}}_1)(\underline{\boldsymbol{U}}_{4\times4} \otimes \underline{\mathbf{I}}_{4\times4})(\underline{\mathbf{I}}_{4\times4} \otimes \underline{\boldsymbol{U}}_1) + \underline{\boldsymbol{U}}_{4\times4} \otimes \underline{\mathbf{I}}_{4\times4}$$

$$\frac{\partial \boldsymbol{P}_v}{\partial \underline{\boldsymbol{A}}_v} = (\underline{\mathbf{I}}_{16\times16} \otimes \underline{\boldsymbol{A}}_v^{-1})\underline{\boldsymbol{U}}_{16\times16}(\underline{\mathbf{I}}_{16\times16} \otimes \underline{\boldsymbol{A}}_v^{-1})(\underline{\mathbf{I}}_{16\times16} \otimes \boldsymbol{Q}_v) \tag{11}$$

$$\frac{\partial \underline{\boldsymbol{P}}}{\partial \underline{\boldsymbol{Q}}} = T_1((-\underline{\boldsymbol{A}}_v^{-1})^T) \tag{12}$$

The first step in generalizing the method is to find the partial derivative of the critical value for the case in which the nonlinear system is tracking the reference dynamics [shown in Eq. (8)] in terms of $\underline{\boldsymbol{A}}_d$. First, the partial derivative of ψ in terms of $\underline{\boldsymbol{A}}_d$ is found using the matrix derivative product rule found in [11], yielding

$$\frac{\partial \psi(\underline{\boldsymbol{A}}_d)}{\partial \underline{\boldsymbol{A}}_d} = \underline{\boldsymbol{U}}_{16\times16}(\underline{\mathbf{I}}_{4\times4} \otimes \boldsymbol{x}) \tag{13}$$

Using again the matrix product rule, the partial derivative of η in terms of $\underline{\boldsymbol{P}}$ is found to be

$$\frac{\partial \eta(\underline{\boldsymbol{P}})}{\partial \underline{\boldsymbol{P}}} = (\underline{\mathbf{I}}_{4\times4} \otimes \boldsymbol{e}^T)\underline{\boldsymbol{U}}_{16\times16}\left(\underline{\mathbf{I}}_{4\times4} \otimes \frac{\underline{\mathbf{I}}_{4\times4}}{|\boldsymbol{e}^T \underline{\boldsymbol{P}} \boldsymbol{B}|}\right) - (\underline{\mathbf{I}}_{4\times4} \otimes \boldsymbol{e}^T \underline{\boldsymbol{P}})\left[\frac{(\boldsymbol{e}^T \underline{\boldsymbol{P}} \boldsymbol{B})(\boldsymbol{e}^T \boldsymbol{B})}{|\boldsymbol{e}^T \underline{\boldsymbol{P}} \boldsymbol{B}|^3}\right] \tag{14}$$

Subsequently, using the matrix chain rule defined in [11], the partial derivative of η in terms of $\underline{\boldsymbol{A}}_d$ is found to be

$$\frac{\partial \eta(\underline{\boldsymbol{P}})}{\partial \underline{\boldsymbol{A}}_d} = T_3^{-1}\left(\frac{\partial \underline{\boldsymbol{P}}}{\partial \underline{\boldsymbol{A}}_d}\right)\left[\underline{\mathbf{I}}_{4\times4} \otimes T_1^{-1}\left(\frac{\partial \eta(\underline{\boldsymbol{P}})}{\partial \underline{\boldsymbol{P}}}\right)\right] \tag{15}$$

Finally, using the matrix product rule and Eqs. (11, 13–15), the general partial derivative of the critical value in terms of $\underline{\boldsymbol{A}}_d$ is found to be

$$\frac{\partial a_{D\text{crit}}}{\partial \underline{\boldsymbol{A}}_d} = T_3^{-1}\left(\frac{\partial \underline{\boldsymbol{P}}}{\partial \underline{\boldsymbol{A}}_d}\right)\left[\underline{\mathbf{I}}_{4\times4} \otimes T_1^{-1}\left(\frac{\partial \eta(\underline{\boldsymbol{P}})}{\partial \underline{\boldsymbol{P}}}\right)\right] \times [\underline{\mathbf{I}}_{4\times4} \otimes (\underline{\boldsymbol{A}}_d \boldsymbol{x} - \boldsymbol{f}(\boldsymbol{x}) + \boldsymbol{B}u_d)] + \left[\underline{\mathbf{I}}_{4\times4} \otimes \frac{\boldsymbol{e}^T \underline{\boldsymbol{P}}}{|\boldsymbol{e}^T \underline{\boldsymbol{P}} \boldsymbol{B}|}\right]\underline{\boldsymbol{U}}_{16\times16}(\underline{\mathbf{I}}_{4\times4} \otimes \boldsymbol{x}) \tag{16}$$

The second step for generalizing the method is to find the partial derivative of the critical value shown in Eq. (8) in terms of $\underline{\boldsymbol{Q}}$. First, using Eqs. (12) and (14), and the matrix chain rule, the partial derivative of η in terms of $\underline{\boldsymbol{Q}}$ is found:

$$\frac{\partial \eta(\underline{\boldsymbol{P}})}{\partial \underline{\boldsymbol{Q}}} = T_3^{-1}(T_1((-\underline{\boldsymbol{A}}_v^{-1})^T))\left[\underline{\mathbf{I}}_{4\times4} \otimes T_1^{-1}\left(\frac{\partial \eta(\underline{\boldsymbol{P}})}{\partial \underline{\boldsymbol{P}}}\right)\right] \tag{17}$$

The partial derivative of ψ in terms of $\underline{\boldsymbol{Q}}$ is a zero matrix since ψ is not a function of $\underline{\boldsymbol{Q}}$. Finally, using Eq. (17) and the matrix chain rule, the general partial derivative of the critical value in terms of $\underline{\boldsymbol{Q}}$ is found to be

$$\frac{\partial a_{D\text{crit}}}{\partial \underline{\boldsymbol{Q}}} = T_3^{-1}(T_1((-\underline{\boldsymbol{A}}_v^{-1})^T))\left[\underline{\mathbf{I}}_{4\times4} \otimes T_1^{-1}\left(\frac{\partial \eta(\underline{\boldsymbol{P}})}{\partial \underline{\boldsymbol{P}}}\right)\right] \times [\underline{\mathbf{I}}_{4\times4} \otimes (\underline{\boldsymbol{A}}_d \boldsymbol{x} - \boldsymbol{f}(\boldsymbol{x}) + \boldsymbol{B}u_d)] \tag{18}$$

The transformations T_1, T_2, and T_3 and permutations matrices $\underline{\boldsymbol{U}}_{m\times n}$ and $\underline{\boldsymbol{U}}_1$ are the same shown in [8,9]. Equations (16) and (18) are called generalized partial derivatives since they were derived based on the most general expression for the critical value, which corresponds to

the case in which the nonlinear dynamics is tracking the reference dynamics. However, these generalized partial derivatives can also be used for the cases in which the nonlinear dynamics is tracking a desired guidance or being regulated.

D. Adaptive Lyapunov Control Strategy

The adaptation used for matrices $\underline{\boldsymbol{Q}}$ and $\underline{\boldsymbol{A}}_d$ is the same adaptation presented in [8,9], which can be expressed as

$$\frac{\Delta A_{ij}}{\Delta t} = \kappa_A\left[-\text{sign}\left(\frac{\partial a_{D\text{crit}}}{\partial A_{ij}}\right)\delta_A\right],$$
$$\frac{\Delta Q_{ij}}{\Delta t} = \kappa_Q\left[-\text{sign}\left(\frac{\partial a_{D\text{crit}}}{\partial Q_{ij}}\right)\delta_Q\right] \tag{19}$$

where $\delta_A = 10^{-6}$, $\delta_Q = 10^{-6}$ (which are of the same order of magnitude as elements in matrix $\underline{\boldsymbol{A}}_d$), and κ_A and κ_Q are defined by

$$\kappa_A = \begin{cases} 1 & \text{if} \left|\frac{\partial a_{D\text{crit}}}{\partial A_{ij}}\right| > \left|\frac{\partial a_{D\text{crit}}}{\partial A_{kl}}\right| \text{for } i,j \neq k,l \\ 0 & \text{otherwise} \end{cases},$$
$$\kappa_Q = \begin{cases} 1 & \text{if} \left|\frac{\partial a_{D\text{crit}}}{\partial Q_{ij}}\right| > \left|\frac{\partial a_{D\text{crit}}}{\partial Q_{kl}}\right| \text{for } i,j \neq k,l \\ 0 & \text{otherwise} \end{cases} \tag{20}$$

This adaptation uses limited knowledge of the nonlinear dynamics, since it requires the $f(\boldsymbol{x})$ in Eq. (2); however, it does not require any knowledge of the drag acceleration. Adapting matrices $\underline{\boldsymbol{Q}}$ and $\underline{\boldsymbol{A}}_d$ implies adapting matrix $\underline{\boldsymbol{P}}$ [see Eq. (9)] and affecting the control law [Eq. (6)].

IV. Numerical Simulations Results

Numerical simulations are performed using STK's HPOP, including a full gravitational field model (based on spherical harmonics), solar radiation pressure, and variable atmospheric drag using the empirical NRLMSISE-00 model. NRLMSISE-00 is an empirical model that includes variations on the density with altitude, as well as with latitude, longitude, and solar and geomagnetic activity. In the simulations, the adaptive Lyapunov controller using the generalized partial derivatives was compared to a nonadaptive version, i.e., with constant $\underline{\boldsymbol{Q}}$ and $\underline{\boldsymbol{A}}_d$.

Both adaptive and nonadaptive Lyapunov controllers can be implemented in the following configurations:

1) The controller is used to force the nonlinear system to directly track a generated guidance trajectory (used for the fly-around and formation-keeping simulations).

2) The controller forces the nonlinear system to track the trajectory of the reference model that is tracking the generated guidance trajectory (used for the rendezvous simulation).

3) The controller forces the nonlinear system to go to a desired final state (regulation).

One key parameter for the implementation of the controllers is the evaluation frequency for the control law [Eq. (6)]. The control remains constant between two successive evaluation instants. The control frequency is also the sampling frequency for the error $\boldsymbol{e}$ in Eq. (6). In general, short waiting times between actuations (high control frequencies) can give better tracking of the dynamics/trajectory; however, they can also result in chattering in the control action and are more expensive in terms of number of switches in the control (control effort). In contrast, long waiting times (low control frequencies) can result in less actuation but can produce large tracking errors.

In practice, the upper bound for the control frequency is given by the speed at which the drag surfaces can be deployed. If the control frequency is lower than twice the largest frequency in the spacecraft relative dynamics, then the $\boldsymbol{e}$ term in Eq. (6) will not be accurately represented according to Shannon's sampling theorem [12]. Thus, twice the largest frequency in the spacecraft relative dynamics constitutes a lower bound for the control frequency. Using the approximation of linear relative dynamics (the Schweighart and Sedwick dynamics [10]), the largest frequency is $\omega/2\pi$, with ω as the orbital angular velocity, which for the initial orbit of the target (see Table 1) has a value of 0.0011 rad/sec. Applying Shannon's sampling theorem [12] gives a lower bound for the control frequency of $3.5 \cdot 10^{-04}$ Hz. This implies approximately a minimum of two actuation switches over a nominal orbit of 90 min (approximately the orbit's duration at the target's initial altitude). For the cases here studied, this analysis imposes time intervals with constant control not longer than 45 min. Below 45 min, one can choose trading off between control effort (number of opening/closing) and tracking accuracy.

Table 1 Spacecraft parameters

Parameter	Value
Target's inclination, *deg*	98
Target's semimajor axis, km	6778
Target's right ascension of the ascending node, deg	262
Target's argument of perigee, deg	30
Target's true anomaly, deg	25
Target's eccentricity	0
Target's velocity v_s, km/s	7.68
Spacecraft mass m, kg	10
$S_{\min}$ = surface retracted, m^2	0.3409
$S_{\max}$ = surface deployed, m^2	2.8409
C_D	2.2

For the simulations, the change in control configuration [Eq. (6)] and the adaptation [Eqs. (16), (18), and (19)] are performed every 10 min for the rendezvous and every 5 min for the fly around and formation keeping, and STK serves as propagator between control changes. The 10 min waiting time between actuations used for the rendezvous simulation gives the small drag forces enough time to change the orbits of the spacecraft, and it avoids chattering in the control action. The 5 min waiting time used for the fly-around and formation-keeping simulations allows the spacecraft to maintain the equilibrium orbit with smaller tracking errors while it still gives enough time to for the drag to affect the orbits and prevents chattering.

The initial orbital elements of the target (center of the LVLH frame) and other parameters for the numerical simulations are shown in Table 1 (see also [7–9]). The target and chaser spacecraft are assumed to be identical. It should be noted that the altitude of the orbit and the maximum and minimum ballistic coefficients were selected so that differential drag can serve as the control variable, overcoming the other differential forces. Differential drag was previously demonstrated to be a viable orbit control means up to 600 km [12], and variations in the ballistic coefficient equal to or greater than the ones chosen for the simulations presented herein can be found in planned or existing missions (see [13–15]). The chaser's initial relative state is shown in Table 2. For all simulations, the initial $\underline{\boldsymbol{Q}}$ matrix was the identity matrix times 10^{-2}. It should be noted that, according to Lyapunov stability theory, the only restriction on the initial $\underline{\boldsymbol{Q}}$ matrix is that it must be positive definite (see [16]).

The orbits of the target and chaser spacecraft are coplanar; therefore, the position and velocity of the chaser relative to the target on the z direction are assumed to be zero.

A. Fly-Around Maneuver and Formation Keeping

This simulation consists of two stages. In the first stage, the spacecraft perform a fly-around maneuver that ends in an equilibrium relative orbit of the chaser around the target. In the second stage, the spacecraft maintain this formation for over one week. In this

Table 2 Initial conditions in the LVLH frame

Parameter	Rendezvous	Fly-around and formation keeping
x, km	−1	0
Y, km	−2	−4.25
$\dot{x}$, km/s	$4.83 \cdot 10^{-07}$	0
$\dot{y}$, km/s	$1.70 \cdot 10^{-04}$	0

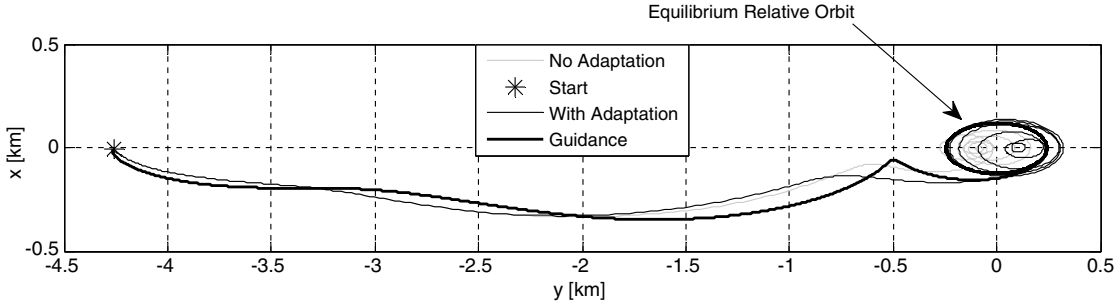

Fig. 1 Fly-around stage and maneuver trajectory.

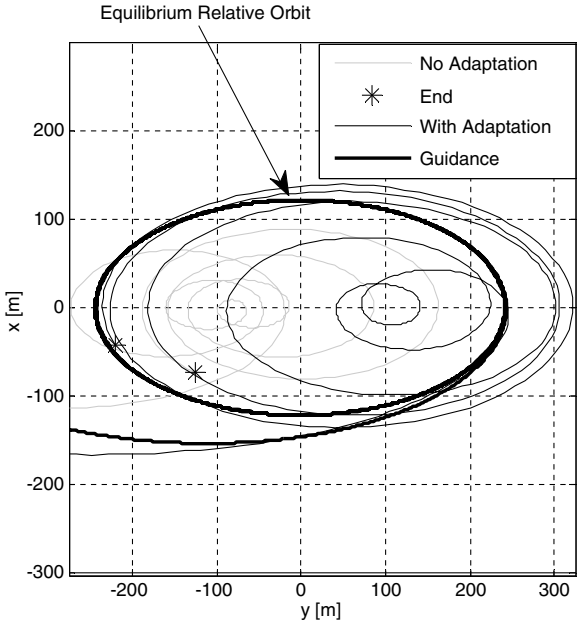

Fig. 2 Fly-around stage, maneuver trajectory, and zoom at the equilibrium relative orbit.

maneuver, both spacecraft start at the same orbit but with a difference in their true anomalies. In the maneuver, the spacecraft follow a guidance in the LVLH plane that leads to the equilibrium relative orbit and then maintains it. This guidance was obtained following the method described in [17]. The simulations end 110 orbital periods (roughly one week) after the guidance reaches the final equilibrium orbit. Both the Lyapunov nonadaptive and adaptive controllers, with the generalized partial derivatives, have been used in these simulations. Figures 1–3 show the trajectories and tracking errors for the first stage of the maneuver until two orbital periods after the spacecraft reached the equilibrium relative orbit. Only two orbital periods are shown to avoid having a congested image. Figure 4 shows the normalized tracking error (the l^2 norm of $\boldsymbol{e}$) for the second stage of the maneuver (formation keeping). For this maneuver, an R_{LQR} value of 10^{18} was chosen, which was found by tuning the nonadaptive controller.

Figures 3 and 4 show that the normalized tracking error is, for the most part, smaller for the adaptive controller than the nonadaptive during the fly-around stage and the formation-keeping stage. Since the fly-around and formation-keeping simulations have the same duration, the mean value of the normalized tracking error can be calculated over the simulations. For the simulation that used the nonadaptive controller, the mean value of the normalized tracking error was 73.78, whereas the one that used the adaptive was 57.47, which represents a reduction of 22.1% by using the adaptive controller.

B. Rendezvous Maneuver

In this maneuver, the spacecraft have an initial difference in both x and y directions. The objective of the maneuver is to drive both relative position and velocity to zero. A guidance trajectory using the method developed in [5] is used. In this simulation, the controller forces the nonlinear system to track the trajectory of the reference model, which is tracking the analytically generated guidance trajectory. To illustrate the importance of the linear stable reference model, two cases for this maneuver were simulated. In case 1, the R_{LQR} value used to obtain the initial $\underline{\boldsymbol{A}}_d$ ($R_{\mathrm{LQR}} = 1.6 \cdot 10^{18}$) yields a linear reference model that has slower dynamics than the actual nonlinear system, whereas in case 2, the selected value ($R_{\mathrm{LQR}} = 1.5 \cdot 10^{17}$)

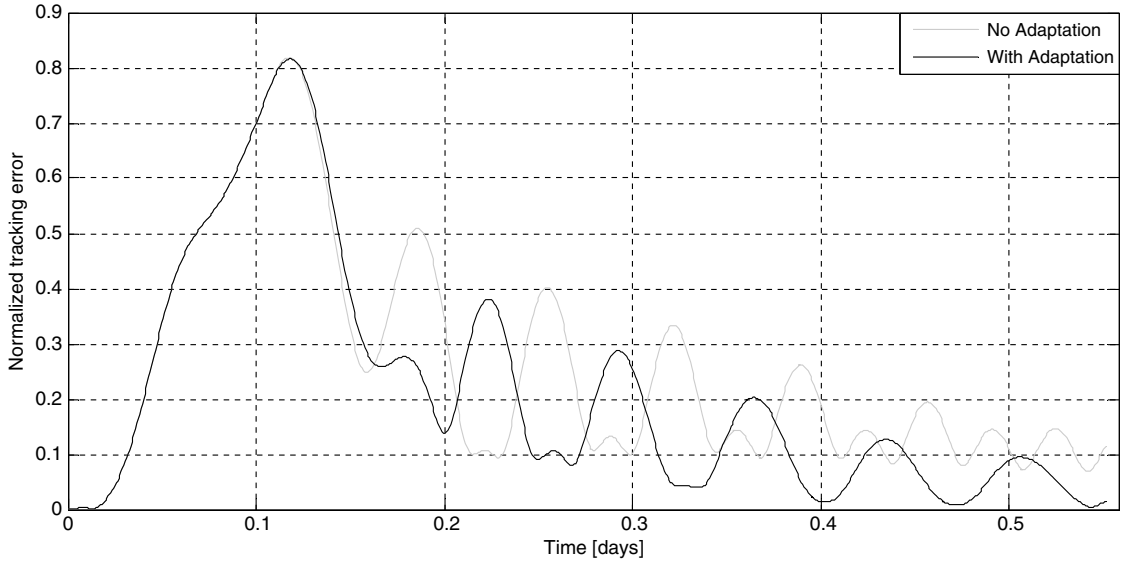

Fig. 3 Fly-around stage and normalized tracking error (the l^2 norm of e).

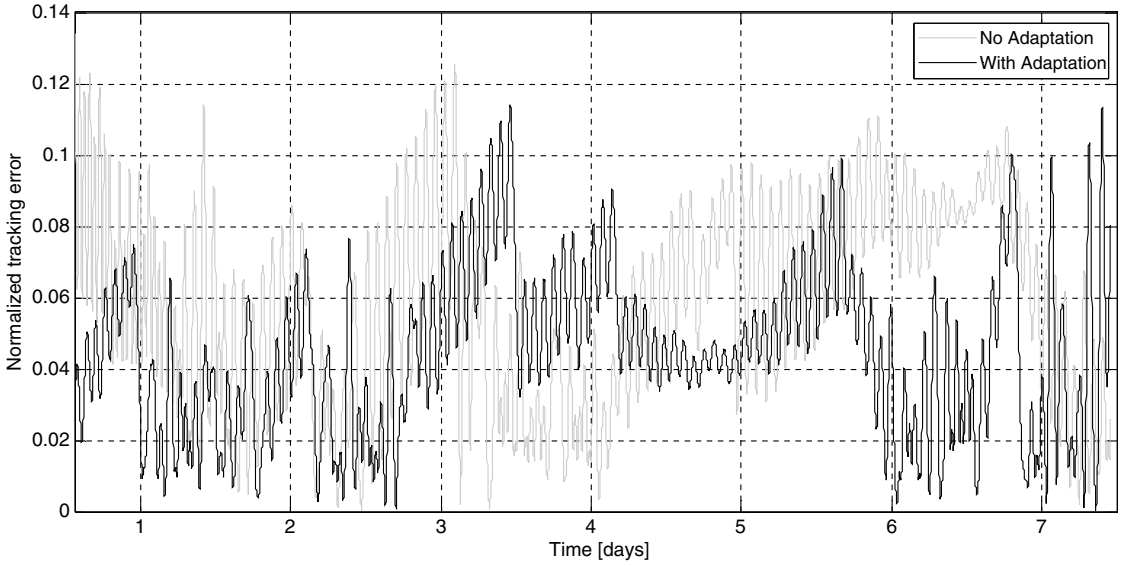

Fig. 4 Formation-keeping stage and normalized tracking error (the l^2 norm of e).

yields a linear reference model that has faster dynamics than the actual nonlinear system. The results of the simulation for this maneuver can be seen in Figs. 5 and 6 for cases 1 and 2, respectively. The maneuver is considered completed when within 10 m from the target.

The normalized errors plots (Figs. 5 and 6, right) show that the adaptive controller allows for maneuvers with shorter durations. Figure 6 (right) shows that, in case 2, the normalized tracking error is, for the most part, smaller for the adaptive controller than the nonadaptive. In contrast, Fig. 5 (right) shows that, in case 1, the normalized tracking error is, for the most part, smaller for the nonadaptive controller than the adaptive. This behavior was not observed in any of the other simulations, in which the use of the adaptive controller resulted in smaller normalized errors during the maneuvers. This anomaly is explained by the fact that the adaptation is designed for reducing the critical value (which, as shown in Eq. (7), is a function of the error among other parameters) and not the error itself; therefore, there can be cases in which the adaptation can result in larger tracking errors, but reducing, on the other hand, the maneuver's duration and control effort when a final point must be reached.

The results also indicate the importance of selecting a reasonable initial linear reference model. As can be seen from the normalized errors plots (see Fig. 5), the linear reference model used for case 1 is easier to track (small normalized error); however, its use results in significantly longer maneuver times. Conversely, the linear reference model used for case 2 converges faster to the rendezvous state, which makes it harder for the controller to track, thus producing a large normalized error (see Fig. 6, right) but a shorter maneuver. Depending on the desired control behavior (better tracking vs. shorter maneuvers), slower or faster linear reference models may be selected.

C. Performance Assessment

The parameters used to evaluate the performance of the controllers are the number of switches in the control, the duration of the maneuver, the means for the critical and actual values of the differential drag acceleration, and the difference between these two values (control margin). The actual value for the differential drag acceleration is available from the atmospheric model used. In practice, this value would not be known a priori; therefore, it is not used by the controller. The trajectories of the spacecraft are different for the two controllers.

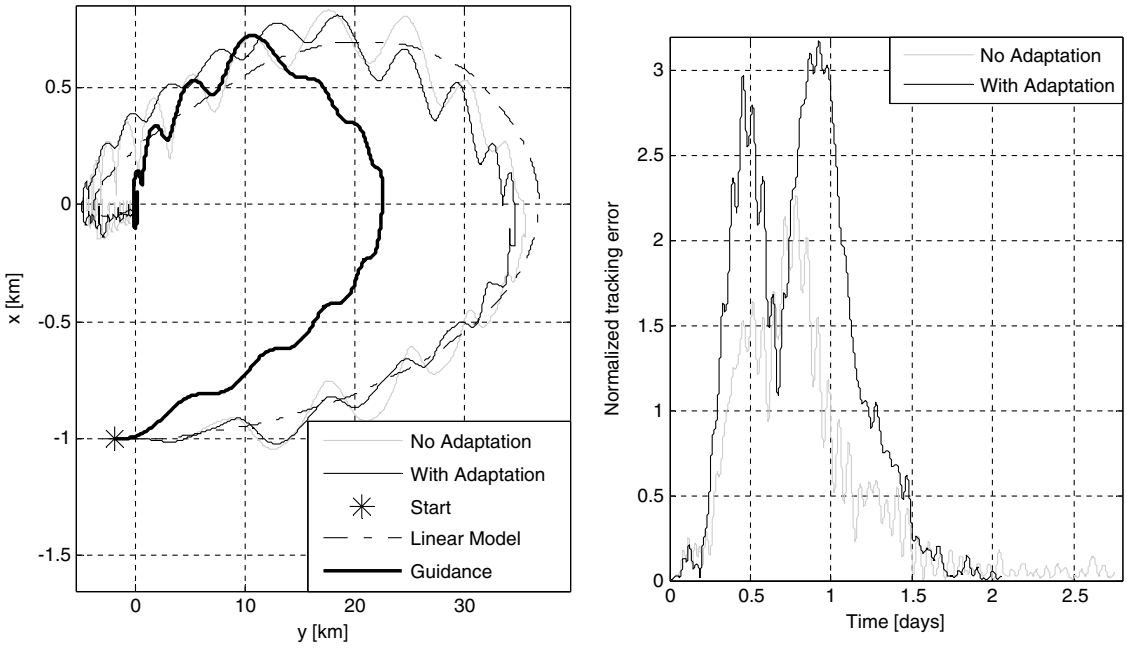

Fig. 5 Rendezvous case 1: maneuver trajectory (left), and tracking errors (right; the l^2 norm of e).

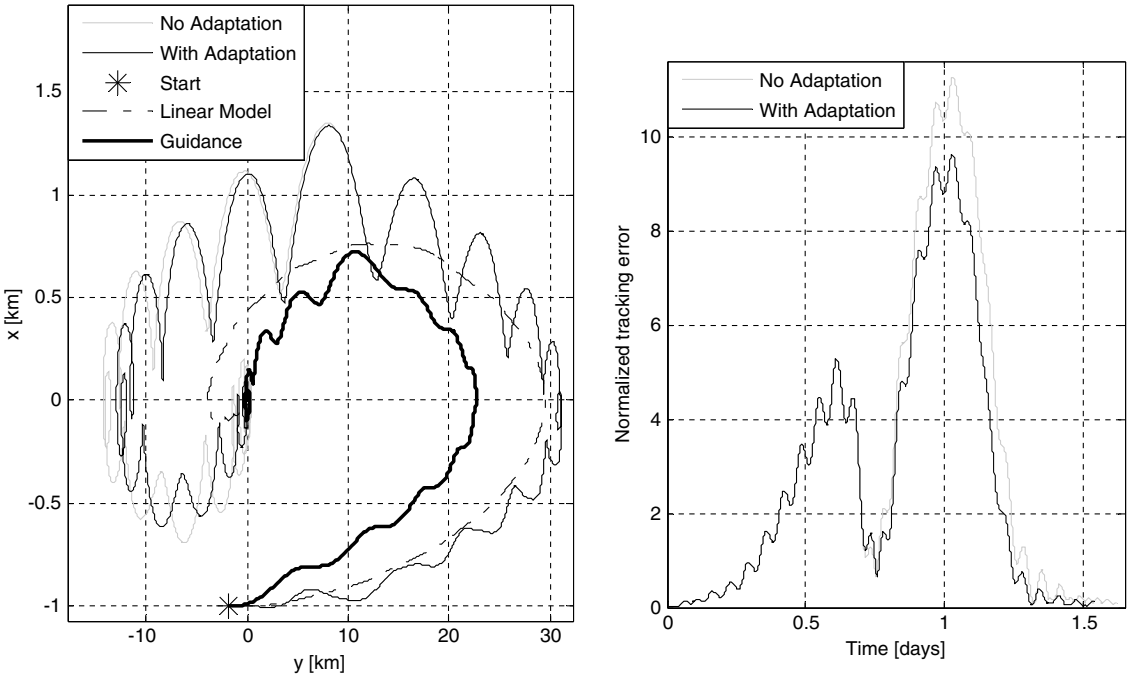

Fig. 6 Rendezvous case 2: maneuver trajectory (left), and tracking errors (the l^2 norm of e).

This means that the spacecraft are flying through slightly different regions of the thermosphere, with different densities. Hence, the control margin is of interest since it subtracts the value of the actual drag acceleration, enabling comparison of trajectories with different densities.

As can be observed from the data in Table 3, the use of the adaptive controller reduced the control effort required to perform the two maneuvers with improvements of 5, 2.6, 48.1, and 2.7% for the fly-around stage, formation-keeping stage, and cases 1 and 2 of the rendezvous maneuvers, respectively. Moreover, the adaptive controller also reduced the duration of the maneuver with improvements of 25.4 and 4.9% for cases 1 and 2 of the rendezvous maneuver, respectively. There was no improvement in duration for the fly around, since the simulation was not ended when within 10 m of the desired final position but after 110 orbital periods when the spacecraft reached the desired equilibrium relative orbit. Additionally, the adaptive controller also was able to increase the control margin with an improvement of 1.6, 0.6, 18.1, and 1.6% for the fly-around stage, formation-keeping stage, and cases 1 and 2 of the rendezvous maneuvers, respectively. As can be seen by comparing the results of case 1 and case 2, the selection of the linear reference model (matrix $\underline{\boldsymbol{A}}_d$) has a substantial impact on the performance of the Lyapunov controller

Table 3 also shows that, for case 1, the actual value of the drag acceleration was lower for the simulation that used the adaptive controller than the one that used the nonadaptive, which indicates that the adaptive controller had, on average, less control force (differential drag acceleration) available to perform the maneuver, although the adaptation still managed to obtain a larger control margin. This explains why this simulation was the only one in which the normalized tracking errors were larger for the adaptive controller than for the nonadaptive. The difference in actual value of the drag accelerations are caused by the differences in the evolution of the orbits of the spacecraft: between the simulations with the adaptive and the nonadaptive controllers.

As previously shown by the authors in [8,9], the implementation of the adaptive controller yields improvements in terms of control effort, maneuver duration, and control margin. Additionally, the use of the general partial derivatives for the adaptation enables more complicated maneuvers beyond those that can be achieved by using regulation. Finally, the critical value is negative on average for all the maneuvers; the critical value can be negative whenever the dynamics of the system are already converging to the desired state.

V. Conclusions

The adaptive Lyapunov feedback controller presented herein enables several planar propellantless spacecraft relative maneuvers using atmospheric differential drag. The controller was successfully used in simulations for a fly-around maneuver followed by a

Table 3 Performance parameters for all simulations

	Tracking trajectory		Tracking dynamics	
Parameter	Stage 1 (fly around)	Stage 2 (formation keeping)	Rendezvous case 1	Rendezvous case 2
		Nonadaptive		
Control changes	80	1877	239	37
Time, h	13.23	179.07	66.05	38.92
Drag mean critical value, m/s^2	$-5.90 \cdot 10^{-6}$	$-1.17 \cdot 10^{-7}$	$-1.16 \cdot 10^{-4}$	$-1.71 \cdot 10^{-4}$
Mean actual drag, m/s^2	$3.37 \cdot 10^{-5}$	$3.85 \cdot 10^{-5}$	$3.56 \cdot 10^{-5}$	$3.50 \cdot 10^{-5}$
Margin, m/s^2	$3.96 \cdot 10^{-5}$	$3.86 \cdot 10^{-5}$	$1.52 \cdot 10^{-4}$	$2.06 \cdot 10^{-4}$
		Adaptive		
Control changes	76	1829	124	36
Time (hr)	13.23	179.07	49.28	37
Drag mean critical value, m/s^2	$-6.24 \cdot 10^{-6}$	$-1.46 \cdot 10^{-7}$	$-1.50 \cdot 10^{-4}$	$-1.74 \cdot 10^{-4}$
Mean actual drag, m/s^2	$3.40 \cdot 10^{-5}$	$3.87 \cdot 10^{-5}$	$3.47 \cdot 10^{-5}$	$3.50 \cdot 10^{-5}$
Margin, m/s^2	$4.03 \cdot 10^{-5}$	$3.88 \cdot 10^{-5}$	$1.85 \cdot 10^{-4}$	$2.09 \cdot 10^{-4}$

formation-keeping period and a rendezvous maneuver. The development of analytical expressions for the general partial derivatives of the differential drag critical value ensuring Lyapunov stability in terms of matrices $\underline{\boldsymbol{Q}}$ and $\underline{\boldsymbol{A}}_d$ (chosen by the control designer, i.e., independent variables), allows for the implementation of the adaptive Lyapunov controller for tracking a trajectory, the dynamics of a reference model, in addition to simply regulating to a desired final state. The adaptation analytically corrects unrealistic initial linear reference dynamics, holding the promise for future onboard implementation on real spacecraft.

The simulations results indicate that the implementation of the adaptive Lyapunov controller allows for smoother maneuvers with less duration, less actuation, greater control margin, and satisfactory accuracy. The use of the general derivatives enables the implementation of the adaptive Lyapunov controller for virtually any relative maneuver confined to the orbital plane. The results also confirm the importance of the linear reference model on the performance of both adaptive and nonadaptive controllers, representing an important topic for further investigation.

References

[1] Leonard, C. L., Hollister, W. M., and Bergmann, E. V., "Orbital Formationkeeping with Differential Drag," *Journal of Guidance, Control, and Dynamics*, Vol. 12, No. 1, 1989, pp. 108–113. doi:10.2514/3.20374

[2] Chang, H. S., Kim, B. W., Lee, C. G., Min, S. L., Choi, Y., Yang, H. S., Kim, D. N., and Kim, C. S., "FSA-Based Link Assignment and Routing in Low-Earth Orbit Satellite Networks," *IEEE Transactions on Vehicular Technology*, Vol. 47, No. 3, 1998, pp. 1037–1048. doi:10.1109/25.704858

[3] Peters, P. N., Gregory, J. C., and Swann, J. T., "Effects on Optical Systems from Interactions with Oxygen Atoms in Low Earth Orbits," *Applied Optics*, Vol. 25, No. 8, 1986, pp. 1290–1298. doi:10.1364/AO.25.001290

[4] Kumar, B. S., and Ng, A., "A Bang–Bang Control Approach to Maneuver Spacecraft in a Formation with Differential Drag," *AIAA Guidance, Navigation and Control Conference and Exhibit*, AIAA Paper 2008-6469, Aug. 2008, doi:10.2514/6.2008-6469

[5] Bevilacqua, R., and Romano, M., "Rendezvous Maneuvers of Multiple Spacecraft by Differential Drag under J_2 Perturbation," *Journal of Guidance, Control, and Dynamics*, Vol. 31, No. 6, 2008, pp. 1595–1607. doi:10.2514/1.36362

[6] Bevilacqua, R., Hall, J. S., and Romano, M., "Multiple Spacecraft Assembly Maneuvers by Differential Drag and Low Thrust Engines," *Celestial Mechanics and Dynamical Astronomy*, Vol. 106, No. 1, 2010, pp. 69–88. doi:10.1007/s10569-009-9240-3

[7] Pérez, D., and Bevilacqua, R., "Lyapunov-Based Spacecraft Rendezvous Maneuvers Using Differential Drag," *AIAA Guidance, Dynamics and Control Conference 2011*, AIAA Paper 2011-6630. doi:10.2514/6.2011-6630

[8] Pérez, D., and Bevilacqua, R., "Differential Drag Spacecraft Rendezvous Using an Adaptive Lyapunov Control Strategy," *1st International Academy of Astronautics Conference on Dynamics and Control of Space Systems*, AIAA, Portland, OR, March 2012; also IAA-AAS Paper DyCoSS1-09-05.

[9] Pérez, D., and Bevilacqua, R., "Differential Drag Spacecraft Rendezvous Using an Adaptive Lyapunov Control Strategy," *Acta Astronautica*, Vol. 83, Feb.–March 2013, pp. 196–207. doi:10.1016/j.actaastro.2012.09.005

[10] Schweighart, S. A., and Sedwick, R. J., "High-Fidelity Linearized J_2 Model for Satellite Formation Flight," *Journal of Guidance, Control, and Dynamics*, Vol. 25, No. 6, 2002, pp. 1073–1080. doi:10.2514/2.4986

[11] Graham, A., *Kronecker Products and Matrix Calculus: With Applications*, Horwood, England, U.K., 1981, pp. 121–125.

[12] Shannon, C. E., "Communication in the Presence of Noise," *Proceedings of the Institute of Radio Engineers*, Vol. 37, No. 1, pp. 10–21, Jan. 1949; also *Proceedings of the IEEE*, Vol. 86, No. 2, Feb. 1998, pp. 447–457.

[13] Mason, C., Tilton, G., Vazirani, N., Spinazola, J., Guglielmo, D., Bevilacqua, R., and Samuel, J., "Origami-Based Drag Sail for CubeSat Propellant-Free Maneuvering," *5th Nano-Satellite Symposium*, The University of Tokyo, Tokyo, Nov. 2013.

[14] Maclay, C. T., "Satellite Station-Keeping of the ORBCOMM Constellation via Active Control of Atmospheric Drag: Operations, Constraints, and Performance," *Advances in Astronautical Sciences*, Vol. 120, Pt. I, 2005, pp. 763–773.

[15] Lambert, C., Kumar, B. S., Hamel, J. F., and Ng, A., "Implementation and Performance of Formation Flying Using Differential Drag," *Acta Astronautica*, Vol. 71, Feb.–March 2012, pp. 68–82. doi:10.1016/j.actaastro.2011.08.013

[16] Gajic, Z., and Qureshi, M. T. J., *Lyapunov Matrix Equation in System Stability and Control*, Courier Dover, New York, 2008, p. 6.

[17] Bevilacqua, R., "Analytical Guidance Solutions for Spacecraft Planar Rephasing via Input Shaping," *Journal of Guidance, Control, and Dynamics*, Vol. 37, No. 3, 2014, pp. 1042–1047, doi:10.2514/1.G000008

This article has been cited by:

1. Salvatore Sarno, Giancarmine Fasano, Marco D'Errico. 2019. Modeling relative motion of LEO satellites at different altitudes. *Acta Astronautica* **156**, 197-207. [Crossref]
2. Danil Ivanov, Uliana Monakhova, Mikhail Ovchinnikov. 2019. Nanosatellites swarm deployment using decentralized differential drag-based control with communicational constraints. *Acta Astronautica* . [Crossref]
3. D. Spiller, Ko Basu, Fabio Curti, Christian Circi. 2018. On the optimal passive formation reconfiguration by using attitude control. *Acta Astronautica* **153**, 259-273. [Crossref]
4. D. Ivanov, M. Kushniruk, M. Ovchinnikov. 2018. Study of satellite formation flying control using differential lift and drag. *Acta Astronautica* **152**, 88-100. [Crossref]
5. Cyrus Foster, James Mason, Vivek Vittaldev, Lawrence Leung, Vincent Beukelaers, Leon Stepan, Rob Zimmerman. 2018. Constellation Phasing with Differential Drag on Planet Labs Satellites. *Journal of Spacecraft and Rockets* **55**:2, 473-483. [Abstract] [Full Text] [PDF] [PDF Plus]
6. Xu Huang, Ye Yan, Zherui Huang. 2017. Finite-time control of underactuated spacecraft hovering. *Control Engineering Practice* **68**, 46-62. [Crossref]
7. Brenton Smith, Russell Boyce, Laurie Brown, Matthew Garratt. 2017. Investigation into the Practicability of Differential Lift-Based Spacecraft Rendezvous. *Journal of Guidance, Control, and Dynamics* **40**:10, 2682-2689. [Citation] [Full Text] [PDF] [PDF Plus]
8. Xu Huang, Ye Yan. 2017. Saturated Backstepping Control of Underactuated Spacecraft Hovering for Formation Flights. *IEEE Transactions on Aerospace and Electronic Systems* **53**:4, 1988-2000. [Crossref]
9. Dario Spiller, Fabio Curti, Christian Circi. 2017. Minimum-Time Reconfiguration Maneuvers of Satellite Formations Using Perturbation Forces. *Journal of Guidance, Control, and Dynamics* **40**:5, 1130-1143. [Abstract] [Full Text] [PDF] [PDF Plus]
10. David Guglielmo, David Pérez, Riccardo Bevilacqua, Leonel Mazal. 2016. Spacecraft relative guidance via spatio-temporal resolution in atmospheric density forecasting. *Acta Astronautica* **129**, 32-43. [Crossref]
11. Ohad Ben-Yaacov, Anatoly Ivantsov, Pini Gurfil. 2016. Covariance analysis of differential drag-based satellite cluster flight. *Acta Astronautica* **123**, 387-396. [Crossref]
12. David Pérez, Riccardo Bevilacqua. 2016. Differential Drag-Based Reference Trajectories for Spacecraft Relative Maneuvering Using Density Forecast. *Journal of Spacecraft and Rockets* **53**:1, 234-239. [Citation] [Full Text] [PDF] [PDF Plus]
13. Gabriella Gaias, Jean-Sébastien Ardaens, Oliver Montenbruck. 2015. Model of $$J_2$$ J 2 perturbed satellite relative motion with time-varying differential drag. *Celestial Mechanics and Dynamical Astronomy* **123**:4, 411-433. [Crossref]
14. David Pérez, Riccardo Bevilacqua. 2015. Neural Network based calibration of atmospheric density models. *Acta Astronautica* **110**, 58-76. [Crossref]